Lab 4 Navigation with IMU and Magnetometer v1.1

In this study, we utilized the VN-100 Inertial Measurement Unit (IMU) to gather data on acceleration, gyroscope, and magnetometer, and the GPS Receiver to capture positioning information. Our aim was to refine this data to reconstruct the projected path of a vehicle journey in Boston, enabling us to evaluate the precision of both IMU and GPS in pinpointing location.

Test Setup and Data Collection Procedure

For our experiment, we drove around Boston, gathering data simultaneously from the IMU and GPS. Proper placement of these devices was crucial for accurate data collection. The IMU was secured on the car's dashboard, aligned at a zero-degree angle, with its x-axis pointing forward. This was based on the presumption of operating in a 2D plane, with the x-direction aligned with the vehicle's path. Concurrently, the GPS was positioned above and aligned with the IMU, ensuring minimal obstructions for GPS signals and alignment of data sets from both devices.

Data Analysis Methodology

Our analysis involved examining the data from the ROS topics to identify and correct key parameters describing the vehicle's motion. The subsequent sections detail plots and interpretations derived from this data analysis.

Magnetometer Correction

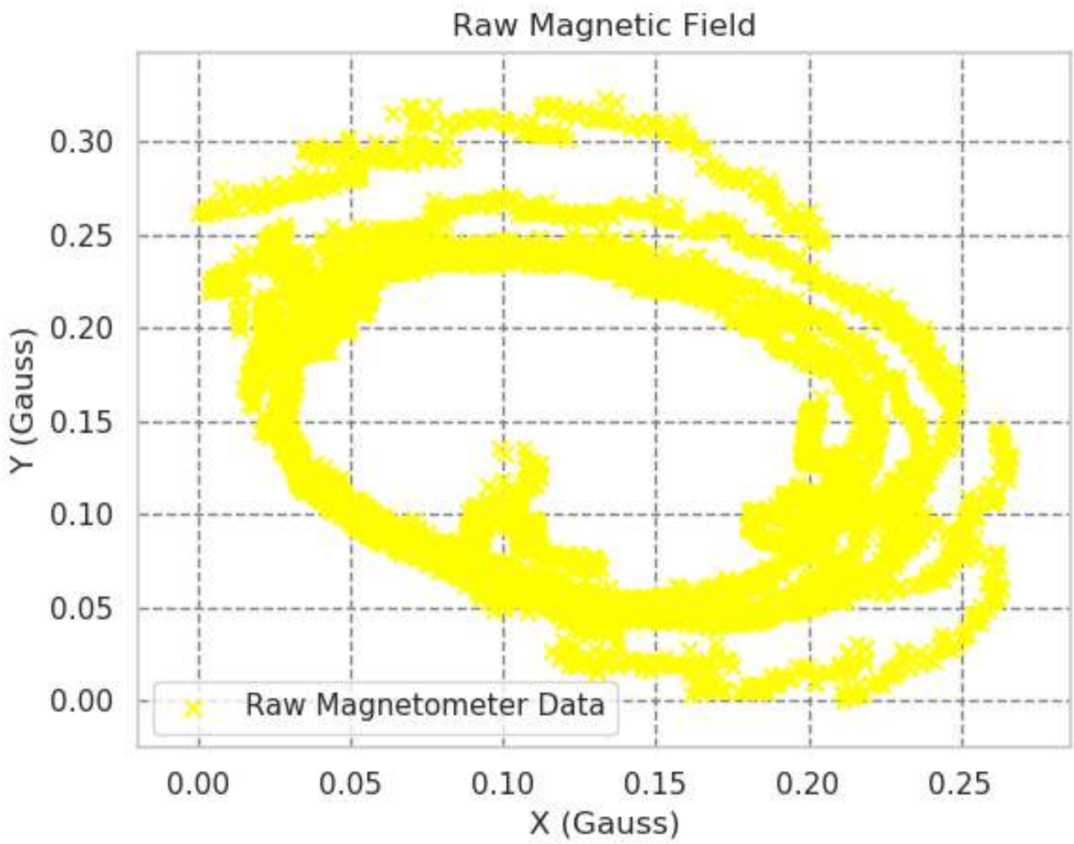

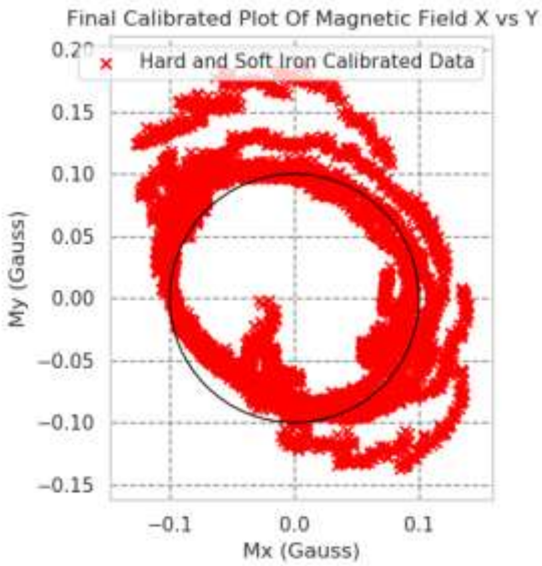

The calibration process involved collecting raw magnetometer data while rotating the sensor through multiple orientations. This provided a comprehensive dataset that reflected the full scope of magnetic interference experienced by the sensor.

Hard-Iron Distortion

Hard-iron distortions, caused by permanent magnetic fields in the sensor's environment, were evident in the data as a consistent offset from the origin. The calibration process corrected this by identifying and subtracting the average bias from all measurements.

Soft-Iron Distortion

Soft-iron distortions, which result from interactions with non-permanent or induced magnetic fields, typically distort the magnetometer's readings into an elliptical shape. The calibration adjusted these distortions by scaling the data along the principal axes of the observed ellipse, effectively reshaping it into a circle.

Estimation of Yaw Angle from Magnetometer Data

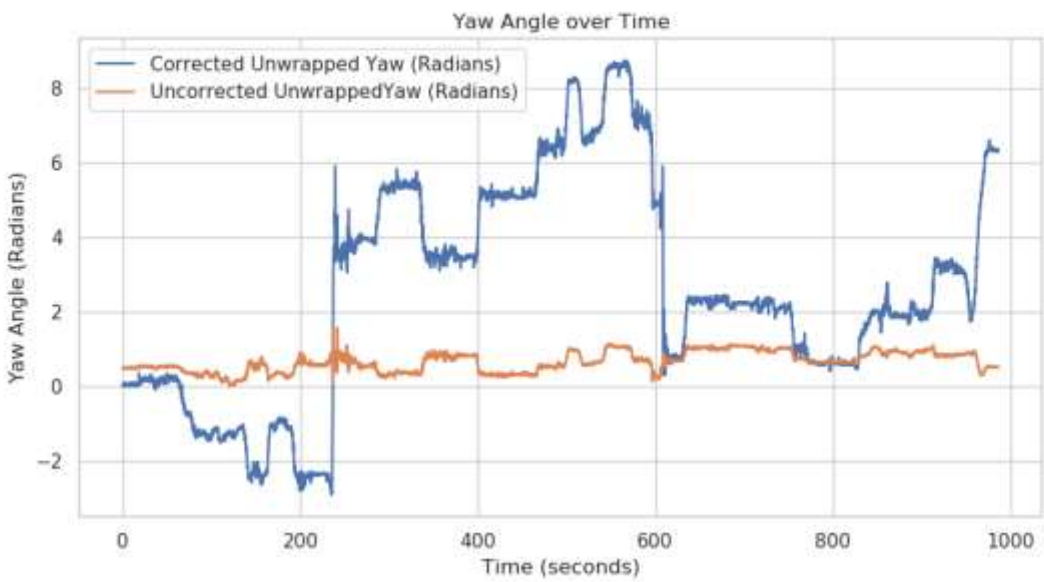

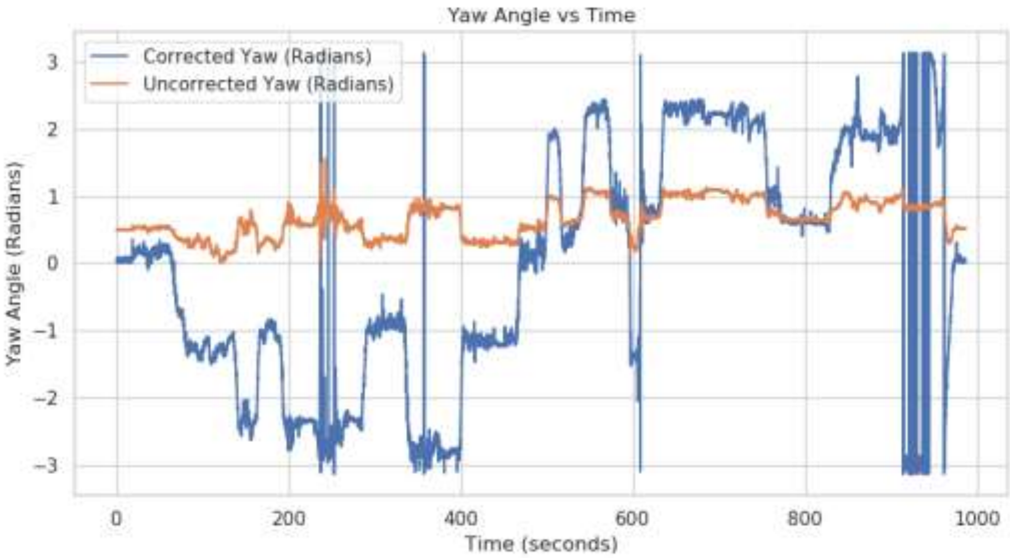

Yaw Angle vs Time
Corrected Yaw (Radians)
Uncorrected Yaw (Radians)
Yaw Angle (Radians)
Time (seconds)

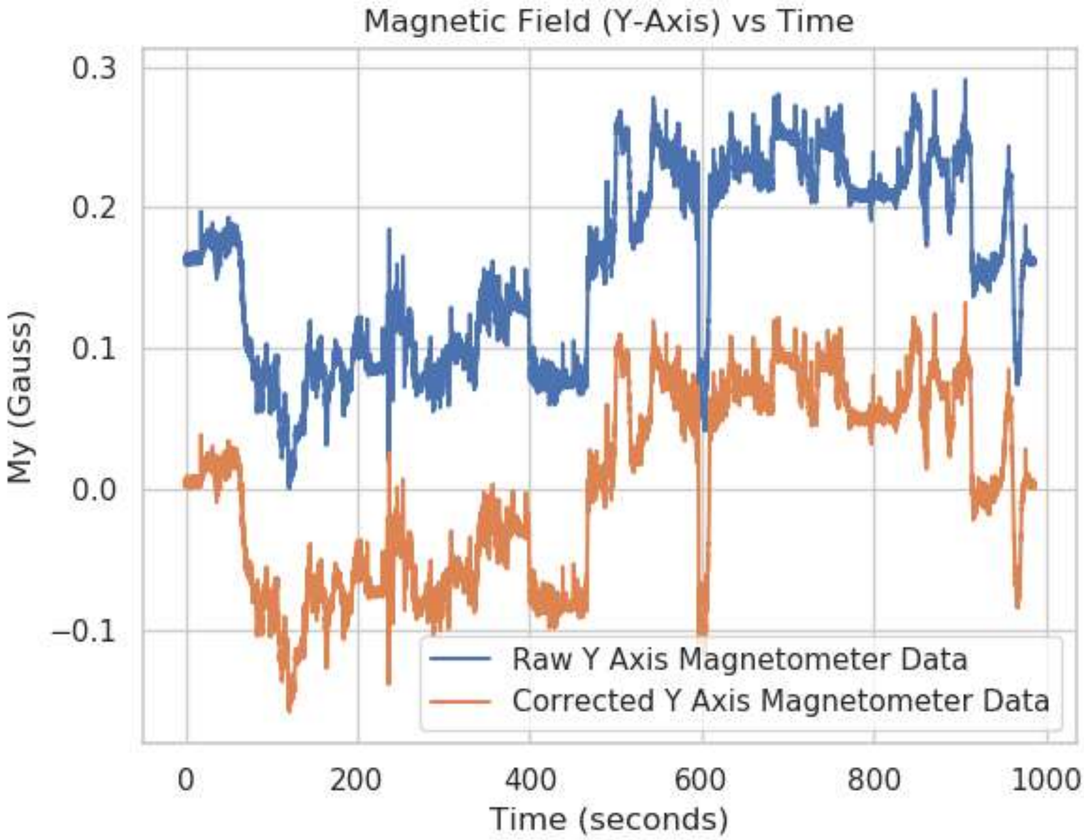

Magnetic Field (Y-Axis) vs Time
Raw Y Axis Magnetometer Data
Corrected Y Axis Magnetometer Data
My (Gauss)
Time (seconds)

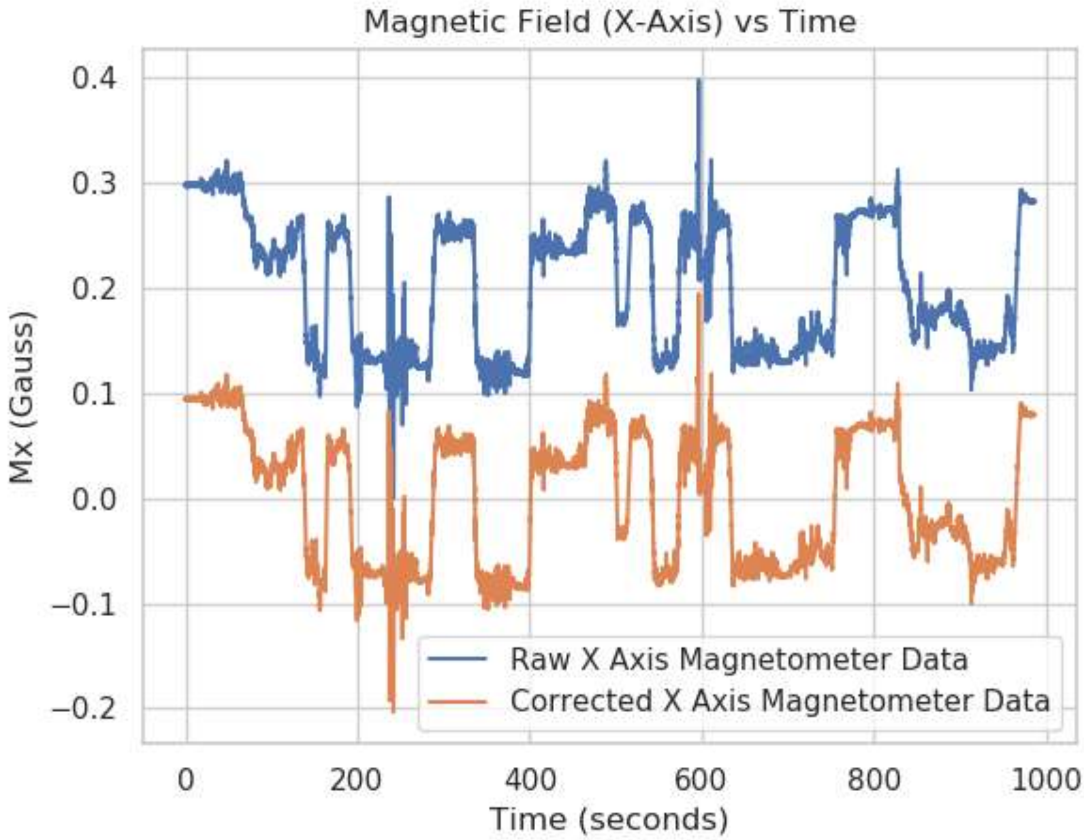

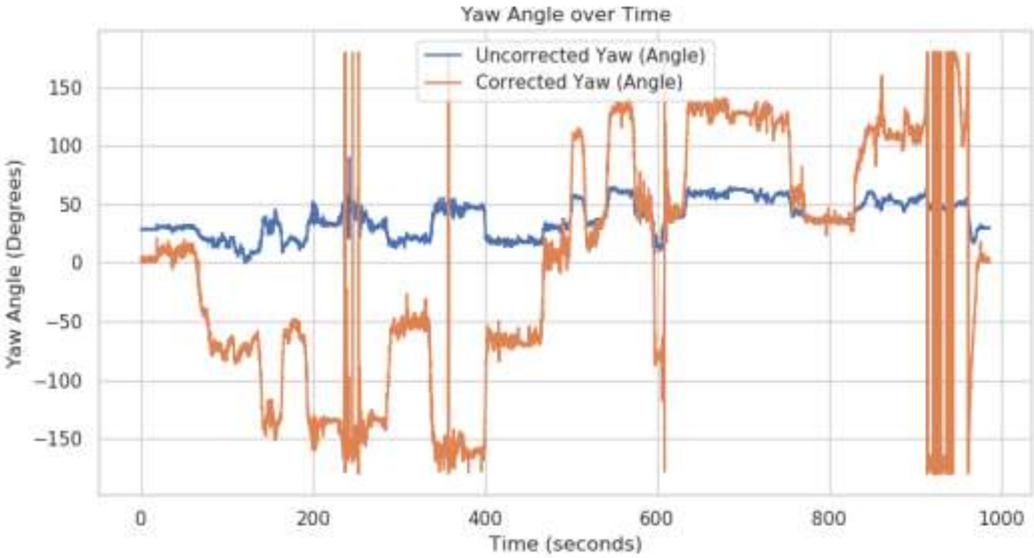

Magnetometer Data Analysis

The magnetometer's raw and calibrated X and Y-axis data over time were analysed to observe the effect of calibration on the sensor's readings. Figures 1 and 2 show the magnetic field's variation with respect to time for both the X and Y axes.

These figures illustrate that the calibration process significantly stabilized the magnetometer's readings, particularly notable in the comparison between the raw and corrected data.

Yaw Angle Estimation

Yaw angle estimation was performed using both the raw and calibrated magnetometer data. The yaw angle over time, both corrected and uncorrected, was plotted to visualize the effect of calibration.

Figures 3, 4, and 5 present the yaw angles derived from the magnetometer's data before and after calibration. The unwrapped plots (Figure 4) display continuous angle data, removing the artificial discontinuities caused by wrapping at $\pm\pi$ radians. Additionally, Figure 5 shows the yaw angle in degrees, providing an alternative perspective for analysis.

The comparison between the uncorrected and corrected yaw angles reveals the significance of calibration. The corrected data follows a smoother and more consistent pattern, suggesting that the calibration process has effectively reduced noise and corrected systematic errors. This improvement is crucial for applications relying on precise heading information.

The unwrapped yaw angle plots (Figures 4 and 5) are particularly insightful, as they show the true continuous rotation without reset points that can obscure trends and patterns in the data.

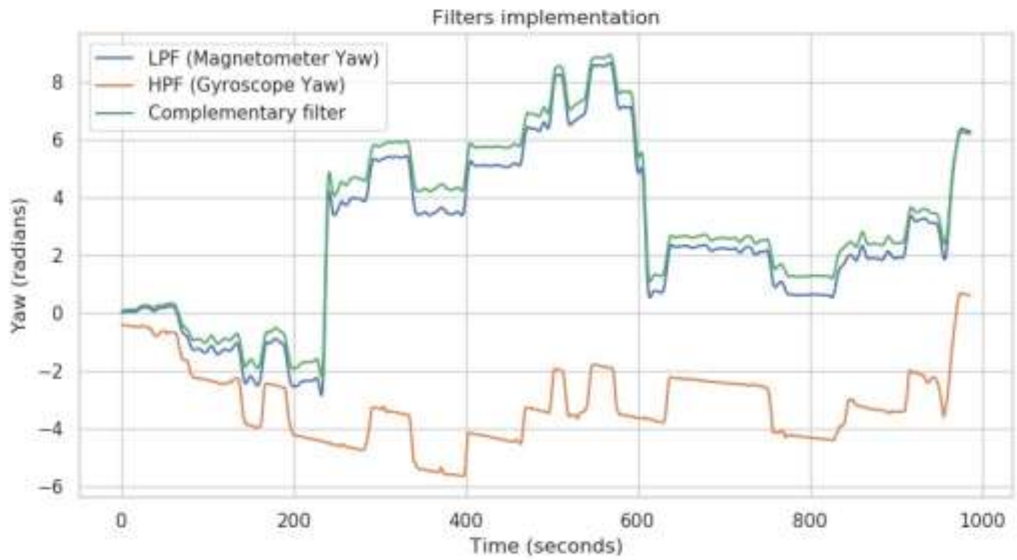

Low Pass Filter (Magnetometer), High Pass Filter (Gyroscope) & Complementary Filter

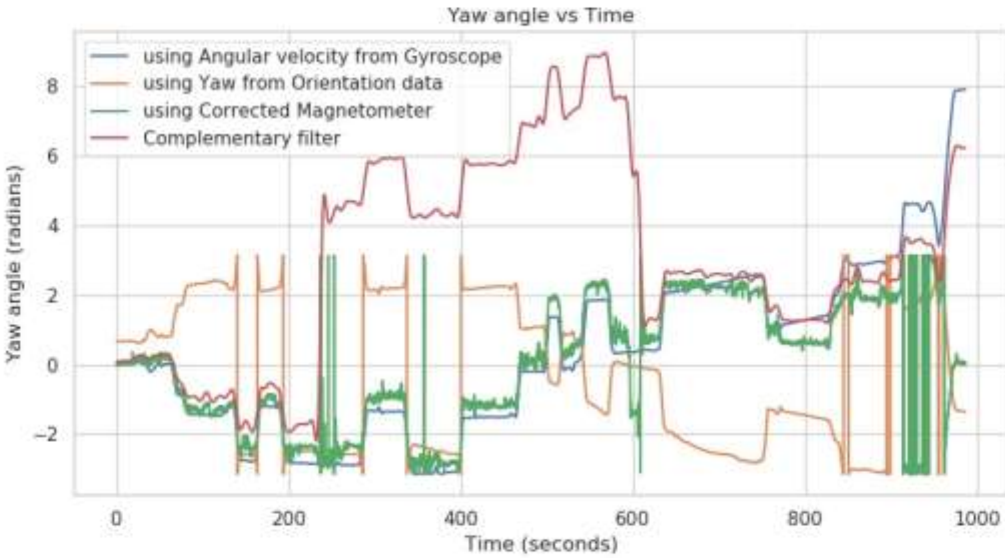

Comparison of Yaw angle from Gyroscope, Orientation (by IMU), Magnetometer, and Complementary Filter

The yaw calculated using the magnetometer is passed onto a Low Pass Filter (LPF) and the yaw estimated using the Gyroscope is passed onto a High Pass Filter (HPF). The outputs of these two filters are combined to form a singular component as the Complementary Filter. The cut-off frequencies were chosen as 0.1 and 0.0001 for the LPF and HPF.
The yaw estimate resulting from the complementary filter would be preferred for use in a system with complex functionalities which has requirements for very accurate estimation

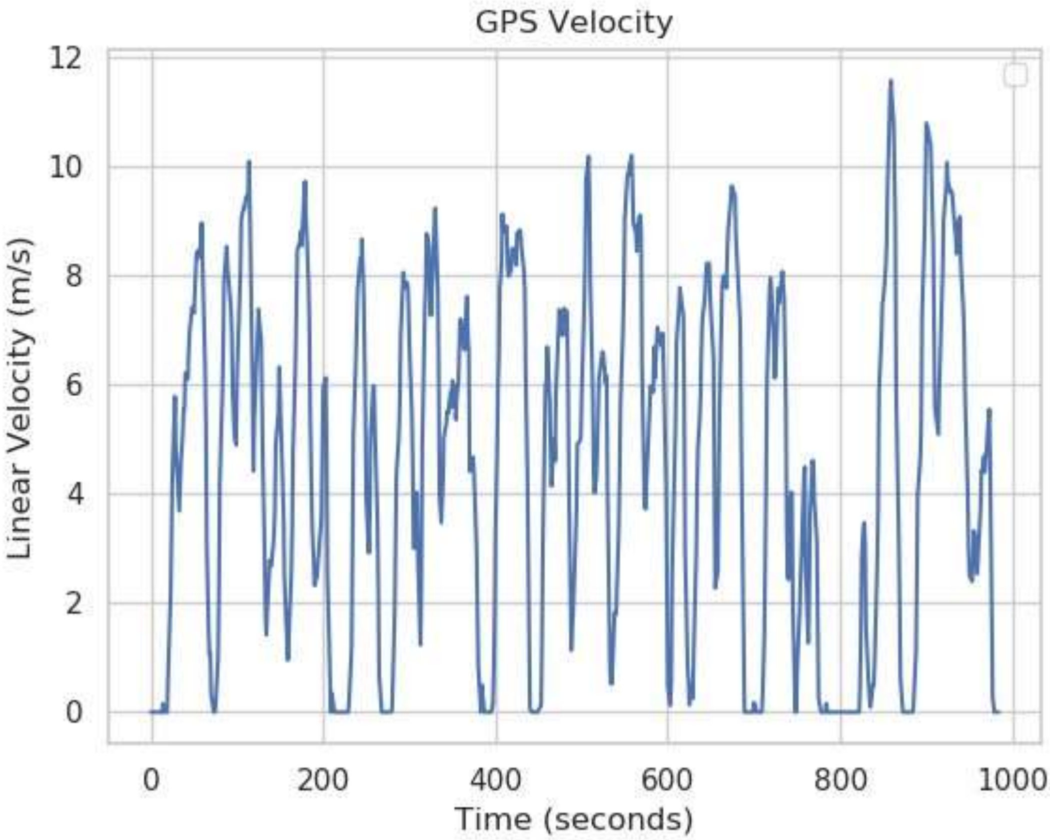

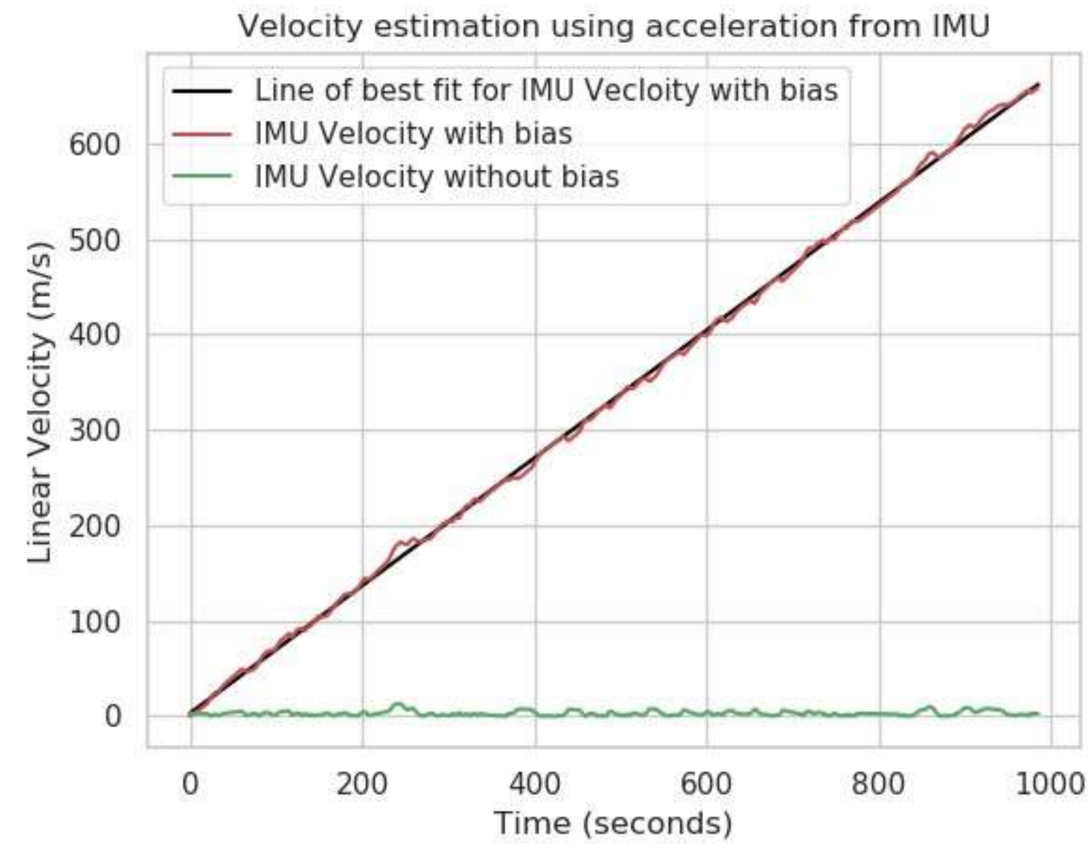
Velocity estimation using acceleration from IMU
Line of best fit for IMU Vecloity with bias
IMU Velocity with bias
IMU Velocity without bias
Linear Velocity (m/s)
0
100
200
300
400
500
600
0
200
400
600
800
1000
Time (seconds)

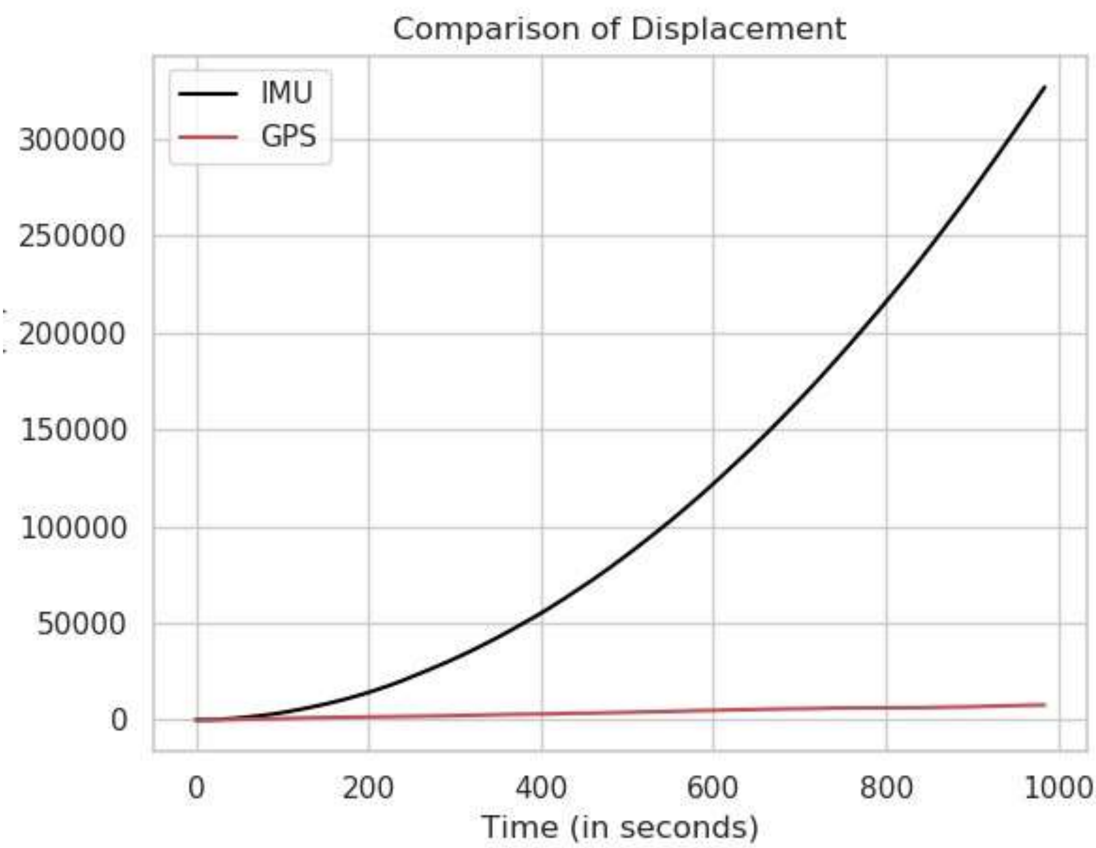
Comparison of Displacement
IMU
GPS
0
50000
100000
150000
200000
250000
300000
0
200
400
600
800
1000
Time (in seconds)

The adjustments included fitting the raw data into a linear line and using this fit line as the new dataset for further calculations. Moreover, the absolute values of the points from this new fit line were considered. The discrepancies present in the velocity estimate between accel, and GPS are primarily that the one from IMU being a cumulative sum as it is obtained by integration of acceleration values over the complete duration of driving.

Velocity and Displacement Estimation

Figure 9 shows the GPS-derived velocity, illustrating variations over time that correspond to the vehicle's motion. The data, however, is noisy, potentially due to GPS signal fluctuations.

Figure 10 demonstrates the estimation of velocity using acceleration data from the IMU. The plot includes a bias-corrected and an uncorrected line, along with a line of best fit. The bias-corrected velocity closely matches the line of best fit, indicating a successful correction of initial acceleration bias.

Figure 11 contrasts the displacement estimated from the IMU and the GPS data. The IMU's displacement shows a steep increase over time, deviating significantly from the GPS data, which remains relatively constant. This discrepancy is likely due to the accumulation of error in the IMU data integration process.